Research Article

Nano Biomed Eng

Silver Nanoparticles Derived from *Artocarpus heterophyllus* for Antimicrobial Nano-gels: A Green Synthesis Approach

Rohankumar R. Chavan[1,2], Mangesh A. Bhutkar[3], Vishal H. Thorat[4], Somnath D. Bhinge[5]

[1] Research scholar, Rajarambapu College of Pharmacy, Kasegaon, Maharashtra 415404, India
[2] Department of Pharmaceutical Chemistry, Bharati Vidyapeeth College of Pharmacy, Kolhapur, Maharashtra 416013, India
[3] Department of Pharmaceutics Rajarambapu College of Pharmacy, Kasegaon, Maharashtra 415404, India
[4] Department of Pharmacognosy, Bharati Vidyapeeth College of Pharmacy, Kolhapur, Maharashtra 416013, India
[5] Department of Pharmaceutical Chemistry Rajarambapu College of Pharmacy, Kasegaon, Maharashtra 415404, India

Corresponding author. E-mails: rohankumar3102@gmail.com, rohankumar.chavan@bharatividyapeeth.edu

Received: Aug. 26, 2024; **Revised:** Oct. 3, 2024; **Accepted:** Oct. 10, 2024

Citation: R.R. Chavan, M.A. Bhutkar, V.H. Thorat, et al. Silver nanoparticles derived from *Artocarpus heterophyllus* for antimicrobial nano-gels: a green synthesis approach. *Nano Biomedicine and Engineering*, 2024, 16(4): 638−651.

http://doi.org/10.26599/NBE.2024.9290104

Abstract

Artocarpus heterophyllus, commonly known as jackfruit, is widely valued for its nutritional benefits, with its leaf extract being studied for various medicinal properties. The synthesis of nanoparticles from *A. heterophyllus* leaf extract utilizes it natural bioactive compounds while addressing limitations like poor bioavailability, offering a greener and more efficient platform for medicinal delivery. This research aimed to enhance the eco-friendly production of silver nanoparticles (AH-AgNPs) from *A. heterophyllus* leaf extract using a Design of Experiments approach. The effects of varying concentrations of plant extract and silver nitrate on AH-AgNP size and entrapment efficiency were assessed through analysis of variance. Optimized AH-AgNPs were characterized using ultraviolet (UV)–visible (Vis) and Fourier transform infrared (FT-IR) spectroscopy, as well as SEM and TEM for determining size and shape. A Carbopol 940 gel incorporating AH-AgNP was formulated and evaluated for physicochemical properties and *in vitro* antimicrobial activity. The spherical AH-AgNPs measured 109.2 nm in size with a 90.15% entrapment efficiency, exhibiting broadspectrum antimicrobial properties. The resulting gel was light brown, free of lumps, with a uniform consistency, a nearly neutral pH (6.2 ± 0.2 to 7.1 ± 0.2), and a viscosity range of 2 884 cp to 3 047 cp. Notably, its efficacy against *E. coli* surpassed that of a commercial formulation containing 0.2% w/w silver nitrate, indicating potential for treating pathogenic infections.

Keywords: antimicrobial; nanoparticles; nanogel; optimization; silver

Introduction

Nanotechnology modifies substances at the molecular scale, typically within the range of 1–100 nm, enhancing their mechanical, chemical, and optical properties [1–3]. Nanocarriers are increasingly used to deliver a wide range of drugs for combination therapies, addressing various therapeutic needs [4]. Plant-derived compounds such as alkaloids, flavonoids, tannins, phenolic acids, and saponins facilitate the transformation of silver ions (Ag^{+}) into silver atoms (Ag^{0}), generating harmless nanoparticles at the nanoscale while effectively coating the newly formed silver nanoparticles [5]. Plants offer a cost-

effective, single-step synthesis method that is safe, nontoxic, and scalable, making them an ideal choice for nanoparticle production [6, 7].

Emerging infectious diseases, especially bacterial infections, have become more prevalent over the past decade and are anticipated to continue spreading. Prolonged antibiotic use can result in liver and kidney toxicity while also contributing to the rise of antibiotic-resistant bacterial strains due to extensive use, genetic mutations, and the formation of bacterial biofilms [8, 9]. Silver nanoparticles (AgNPs) demonstrate antimicrobial activity by disrupting microbial metabolic pathways, inhibiting electron transfer processes, generating reactive oxygen species, and interacting with bacterial membranes and cell walls, leading to structural damage and bacterial death [10–13]. AgNPs have recognized for their antibacterial properties for centuries [14]. Additionally, silver nanoparticles possess unique attributes, including potent antimicrobial, antioxidant, and anticancer activities [14–19].

Gels, unlike ointments and creams, offer rapid release of active pharmaceutical ingredients and are highly biocompatible with minimal risk of inflammation. They are easy to apply, require no removal, and have emollient effects, thixotropic properties, and a nongreasy texture. Gels are also water-washable, enabling easy application and removal [20]. According to the U.S. Pharmacopeia (USP), gels are semisolid systems made of a suspension of inorganic particles or large organic molecules interpenetrated by a liquid. Carbopol, a synthetic polymer based on carbomer, is widely used in dermatological applications as a suspending agent, stabilizer, and thickener. Cross-linked carbomer polymers create a microgel structure, with organic amines like triethanolamine facilitating neutralization and microgel formation. [21–23].

The synthesis of nanoparticles using *Artocarpus heterophyllus* (jackfruit) leaf extract harnesses its natural bioactive properties, enhancing its medicinal potential. Although *A. heterophyllus* is known for its nutritional and therapeutic benefits, its bioactive compounds often have poor bioavailability, reducing their effectiveness in direct applications. By synthesizing nanoparticles from the leaf extract, these limitations are addressed, offering a more stable and efficient delivery platform.

To further enhance this delivery system, incorporating these nanoparticles into gels can provide additional benefits. The gels serve as a controlled-release matrix, stabilizing the nanoparticles and preventing aggregation. This ensures sustained and targeted delivery of the bioactive compounds, thereby improving their therapeutic efficacy. Moreover, gel-based systems reduce the potential toxicity associated with free nanoparticles, offering a safer and more effective method for utilizing the medicinal properties of *A. heterophyllus* leaf extract. By combining these elements, the natural advantages of the extract are maximized, resulting in a greener and more sustainable delivery approach for various medicinal applications. Moreover, the use of Carbopol not only imparts the necessary physical properties for an effective gel but also enhances the stability, controlled release, and overall therapeutic potential of the *A. heterophyllus* leaf extract-loaded nanoparticles in the formulation.

Design of Experiments (DoE) is extensively widely utilized in scientific fields, such as analytical chemistry and formulation development, for batch optimization [24–27]. Literature reviews reveal that there have been no prior attempts to enhance the production of AgNPs using leaf extract from *A. heterophyllus*. In this study, the DoE technique, along with Design Expert software, was employed to optimize the production of silver nanoparticles from *A. heterophyllus* leaf extracts (AH-AgNPs). The physicochemical characteristics of AH-AgNPs were analyzed using ultraviolet (UV)–visible (Vis) spectroscopy, X-ray diffraction (XRD), Fourier transform infrared (FT-IR), scanning electron microscope (SEM), and transmission electron microscope (TEM), while their potential antioxidant and antibacterial capabilities were investigated to evaluate their biological significance.

Experimental

Plant sampling, identification, and extract collection

The leaves of *A. heterophyllus* (Family: Moraceae) were collected from Morgiri (Patan), Satara district, Maharashtra, India. Botanical identification was performed by Dr. Vinod B. Shimpale from the Department of Botany at The New College Kolhapur,

India. Voucher specimens were deposited in the herbarium under deposition number B01. The leaves were shade-dried three times and extracted with methanol using soxhlet equipment for an entire day. The resulting extract was then filtered through Whatman No. 1 filter paper and concentrated using a Heidolph Hei-VAP Core rotary evaporator. This unrefined methanolic extract was subsequently utilized in pharmacological research and the production of nanoparticles.

Chemicals

This experiment utilized analytical-grade chemicals. The microbiological media and materials were sourced from Himedia. Silver nitrate, ascorbic acid, gallic acid, phloroglucinol, and DPPH were obtained from the Research Laboratory in Mumbai, Maharashtra.

Microorganism used

The organisms used in this experiment included *Staphylococcus aureus* ATCC 6538, *Bacillus subtilis* ATCC 6051, *Escherichia coli* ATCC 8739, and *Aspergillus niger* ATCC 16880. These cultures were sourced from the National Collection of Industrial Microorganisms located in Pune, Maharashtra, India (411008).

Biogenic synthesis of the silver nanoparticles

The crude extract of *A. heterophyllus* leaves (AHL) was utilized to produce silver nanoparticles (AH-AgNPs). In the synthesis of nanoparticles, silver nitrate served as the silver source, following a modified method based on Prabhu et al. [28]. The concentrations of $AgNO_3$ (μg/mL) and extract (μg/mL) were optimized with DoE version 13 (Stat-Ease Inc., Minneapolis, MN, USA). The reaction mixture was incubated at room temperature for 3–4 h. The formation of nanoparticles was monitored by observing the color change from bright green to dark brown, which was further analyzed using UV–Vis spectroscopy (JASCO 1800). The resulting silver nanoparticles were purified by centrifugation at 10 000 r/min for 25–30 min, followed by drying in a vacuum chamber at 35 °C for 24 h.

In silico parameter optimization

A two-factor, three-level complete factorial design was developed and randomized to test all possible combinations of components. DoE version 13.0 was employed to optimize the conditions, focusing on two key factors: $AgNO_3$ concentration (μg/mL) and AHL extract concentration (μg/mL) [29]. These parameters were set at three different levels, ranging from minimal to maximum values. Nine experimental runs were designed accordingly. Responses were assessed for the particle size (nm) and entrapment efficiency (EE%) of the biosynthesized AH-AgNPs. The collected data were analyzed mathematically, and a quadratic second-order model was selected for analysis of variance (ANOVA) testing. The interaction effects between the independent variables were examined through interaction plots, perturbation plots, and predicted versus actual diagnostic charts. Statistical analysis was used to establish the mathematical relationships between the dependent and independent variables. Ultimately, the conditions optimized for AH-AgNPs biosynthesis were determined through both numerical and graphical optimization approaches.

Synthesis and characterization of the optimized AH-AgNPs

AH-AgNPs were synthesized under optimal conditions and then tested using a UV–Vis double-beam spectrophotometer (JASCO 1800, Japan) with 1 cm quartz cells. The nanoparticles' size and shape were characterized using X-ray diffraction, scanning electron microscopy, and transmission electron microscopy. Both the crude extract and AH-AgNPs were analyzed by FT-IR spectroscopy, with spectra recorded in the range of 4 000–600 cm^{-1}, using 25 scans per spectrum in *T*% mode at room temperature. The instrument employed was a BRUKER ALPHA I from Germany [30].

Drug-excipient compatibility study

Before describing the gels, preformulation studies were conducted to explore potential interactions between AH-AgNPs and Carbopol. The compatibility of Carbopol 940 with AH-AgNPs was evaluated through FT-IR spectral analysis using an FT-IR spectrophotometer (Bruker Alpha II).

Formulation of AH-AgNPs incorporated gel

A gel formulation of the optimized batch of synthesized AH-AgNPs was prepared using Carbopol 940 as the gelling agent, employing a cold mechanical method. First, a colloidal suspension of AH-AgNPs (0.02% w/w) was prepared, after which 1% Carbopol was gradually added to the suspension with continuous stirring. This step was followed by

the addition of a drop of triethanolamine [31]. The resulting gel was packaged in wide-mouthed containers and stored in a cool dark place.

Evaluation of AH-AgNPs gel

The prepared gel was evaluated for various physicochemical parameters, including color, appearance, homogeneity, pH, viscosity, spreadability, zeta potential, extrudability, rheological parameters, *in vitro* diffusion, release kinetic studies, and stability.

Color, appearance, and homogeneity

The formulations were visually inspected to assess their color, appearance, and homogeneity [32].

pH and viscosity

A digital pH meter (Thermocare) was used to measure the pH of the gel. For pH measurement, 1 g of AH-AgNPs gel was mixed with 100 mL of water and stored at 4 °C for 2 h. All measurements were conducted in triplicate, and the averages were recorded [33]. The viscosity of the gel formulations was measured using a Brookfield Viscometer with spindle No. 63 at 200 r/min. Before measurement, the gel samples were allowed to settle for 30 min at (25 ± 1) °C.

Spreadability

The spreadability of the gel formulations was evaluated by measuring the spreading diameter of 1 g of gel placed between two horizontal plates after 1 min, with the upper plate applying a weight of 125 g [34].

Zeta potential

The zeta potential of all formulations was measured using a zeta sizer instrument (Malvern Zeta Sizer, Nano ZS90).

Extrudability

The extrudability of the gel was evaluated by measuring the percentage of gel extruded from the tube under a specific applied load. The formulation was placed in a collapsible tube with a 5 mm tip aperture, and a 50 g weight was applied at the bottom of the tube to force the gel through the aperture. The amount of gel extruded was then weighed, calculated, and recorded to assess its extrudability [35].

Rheological studies

Rheological parameters are essential for determining the usability of the gels, as they should exhibit a consistency that is neither too viscous nor too fluid when dispensed. Steady shear properties and frequency sweep tests were performed using a rheometer (Anton Paar MCR 102) equipped with a cone and plate geometry. The methodology outlined by Sandhu et al. was followed to calculate dynamic rheological parameters [36]. To determine steady shear characteristics, the approach by Park et al., with minor adjustments, was used [37]. The variation in the rheological properties under steady shear was characterized by fitting the data to the power law equation (Eq. (1)).

$$\sigma = K\gamma^n \quad (1)$$

where σ represents shear stress (Pa), γ represents shear rate (s^{-1}), K is the consistency index ($Pa \cdot s^n$), and n is the flow behavior index, calculated via linear regression of the square roots of the shear rate-shear stress data.

Steady shear properties

For ease of application from the tube, the gels should exhibit pseudoplastic or non-Newtonian behavior, where an increase in shear rate reduces the gel's viscosity, a phenomenon known as shear thinning. At the same time, the gels must retain high viscosity to stay in place at the application site [38]. This behavior can be predicted by analyzing the steady shear properties. The gel formulations were evaluated by applying shear rates ranging from 0 to 100 s^{-1} at 25 °C, with parameters such as the consistency index (K), yield stress (τ_0), flow index (n), and R^2 being recorded.

Frequency sweep test

In this test, the angular frequency was incrementally increased from 0.1 to 100 rad/s, and a graph plotting the elastic modulus (G') and the viscous modulus (G") against the angular frequency was generated.

In vitro diffusion

Approximately 1 g of the prepared gel was accurately weighed and placed into a donor compartment (dialysis membrane) for the *in vitro* release study of AH-AgNPs. The release of AgNPs from the Carbopol 940 gel was evaluated using a dialysis membrane as the donor compartment, into which the gel containing 1 g of AgNPs was introduced. The dialysis bag was then immersed in 20 mL of deionized water, adjusted to pH 6, within a beaker serving as the receptor

compartment. The temperature was maintained at (37 ± 1) °C, and the receptor solution was continuously stirred at 100 r/min using a magnetic stirrer. Samples of 2 mL were withdrawn at intervals of 0, 0.5, 1, 2, 3, 4, 5, 6, 7, and 8 h, and each withdrawn sample was replaced with fresh medium. The concentration of AgNPs in the collected samples was determined by measuring the absorbance at 430 nm [39].

Release kinetic study

Various kinetic models are available to describe drug release from dosage forms. Developing approaches that reduce the need for bio-studies and streamline product development is advantageous, as changes in formulation quality and quantity can affect drug release and *in vivo* performance [40]. The results from the AH-AgNPs release tests in the gel formulations were fitted to several kinetic equations, including zero-order, first-order, the Higuchi model, and the Korsmeyer–Peppas model.

Stability

The gel formulation was packaged in collapsible tubes and stored at (40 ± 2) °C and 75% ± 5% relative humidity (RH) according to the guidelines of the International Conference on Harmonization. Over a 6-month period, samples were analyzed monthly for color, homogeneity, pH, and zeta potential using the previously described methods [41, 42].

Skin irritation study

Hair from the dorsal side of the rats was completely removed using hair clippers and electric scissors. The shaved area was then cleaned with surgical spirit before applying the gels over a 1.0 cm^2 area of the skin. The rats were observed for 48 h. This study was approved by the Bharati Vidyapeeth College of Pharmacy, Kolhapur, MS, India, in accordance with the guidelines of the Committee for the Purpose of Control and Supervision on Experiments on Animals (CPCSEA) (Reg. No. 988/c/PO/06/CPCSEA).

Antimicrobial activity of the gel

The prepared formulations were evaluated for antimicrobial efficacy against various bacteria (*S. aureus*, *B. subtilis*, and *E. coli*) and fungi (*A. niger*) and compared with a marketed formulation, Silverex M (containing 0.2% w/w silver nitrate). Bacterial strains were cultured in tryptone broth and incubated for 24 h at 37 °C, while fungal spore suspensions were grown in potato dextrose broth and incubated for 5–7 days at room temperature. Bacterial strains were inoculated on SCDA plates and fungi on PDA plates. Wells with an 8 mm diameter were loaded with 10 µL of AH-AgNPs gel (0.2% w/w) and Silverex M gel. The plates were then incubated for 24 h at 37 °C for bacteria and for 2–3 days at room temperature for fungi. After incubation, the inhibition zones around the wells were observed and compared with those of the marketed gel [43].

Results and Discussion

The extract of *A. heterophyllus* leaves (AHL) was mixed with a solution of $AgNO_3$ in a 1∶1 ratio at a concentration of 10 µg/mL. The reaction mixture rapidly changed from colorless to brownish yellow, and within 30 min, the color deepened to brown. This brownish-yellow color is characteristic of AH-AgNPs in aqueous solution and is attributed to their surface plasmon resonance vibrations [44]. The phytochemicals present in the extract likely played a role in facilitating the reduction of silver ions.

Optimization and evaluation of dependent variables

To achieve AH-AgNPs with minimal size and optimal stability, response surface methodology was utilized for statistical process optimization. A full factorial experimental design, incorporating two independent variables at two levels each, was employed to evaluate their impact on the dependent variables. Table 1 displays the transformed values and responses of all the batches. Statistical analysis was conducted to establish the mathematical relationships between the dependent and independent variables. The resulting polynomial equations are presented below:

$$Y_1 = +110.34 + 4.72A + 1.83B - 0.250\,0AB - 1.32A^2 + 0.1333B^2 \quad (2)$$

$$Y_2 = +92.28 + 5.88A + 1.97B - 0.022\,5AB - 0.978\,3A^2 - 0.028\,3B^2 \quad (3)$$

where Y_1 represents the response variable of particle size, while Y_2 denotes the entrapment efficiency. Variables A, B, A^2, and B^2 are the independent factors. Analysis of the polynomial equations enables inference based on the numerical sign and magnitude of the coefficients. The correlation coefficients (r^2) for particle size and entrapment efficiency were determined to be 0.995 2 and 0.986 9, respectively,

Table 1 Factorial batches of silver nanoparticles EE% and particle size.

Std.	Run	Factor 1	Factor 2	Response 1	Response 2
		A: Concentration of extract (mg/mL)	B: Concentration of $AgNO_3$ (mg/mL)	Particle size (nm)	EE%
7	1	1	10	106.4	87.2%
2	2	5.5	1	108.3	89.6%
8	3	5.5	10	112.5	94.7%
5	4	5.5	5.5	110.5	92.47%
4	5	1	5.5	104.3	85.2%
6	6	10	5.5	113.6	97.2%
1	7	1	1	102.5	83.8%
3	8	10	1	112.5	95.48%
9	9	10	10	115.4	98.79%

indicating a strong model fit. The negative coefficients for *A* and *B* in Eqs. (2) and (3) suggest an antagonistic effect of these variables on particle size. Conversely, the positive coefficients for both A and B in Eqs. (2) and (3) indicate a beneficial effect on entrapment efficiency.

The significance and applicability of the model were evaluated using analysis of variance (ANOVA). Table 2 provides data including the standard error, sum of squares, *F* ratio, and *p* values. As shown in Table 2, the *P* values for the independent variables and ANOVA interactions indicate a significant effect on both particle size and entrapment efficiency. The three-dimensional (3D) plots illustrate the varying responses as the two factors change from low to high levels. These maps display how the response surface curves at different component levels, emphasizing key areas by displaying predicted response values. Figure 1 presents graphs for particle size and entrapment efficiency in both two-dimensional (2D) and 3D formats, along with contour plots.

Optimization of the AH-AgNPs Batch

The batch with the highest desirability function value, indicating optimal condition, was selected. The optimal parameters for synthesizing AH-AgNPs were determined to be an $AgNO_3$ concentration of 6.7 μg/mL and an AHL extract concentration of 4.7 μg/mL. Under these conditions, the predicted particle size was 110 nm, with an entrapment efficiency of 91.75% for the synthesized AH-AgNPs.

Validation studies were then conducted on the optimized AH-AgNPs, resulting in observed values of 109.2 nm for particle size and 90.15% for entrapment efficiency. These observed values closely aligned with the predicted responses, exhibiting a prediction error within ±10%, thereby confirming the accuracy of the chosen design and mathematical model.

Characterization of AH-AgNPs using FT-IR, XRD, SEM, and TEM

FT-IR analysis was conducted to identify the bonds and functional groups present in the AHL extract

Table 2 Summary of results from the analysis of variance (ANOVA).

		Particle size					Entrapment efficiency			
Source	df	SS	MS	*F*	*P*	df	SS	MS	*F*	*P*
Model	5	157.40	31.48	335.95	0.000 3	5	232.49	46.50	121.88	0.001 2
A	1	133.48	133.48	1 424.51	<0.000 1	1	207.33	207.33	543.46	0.000 2
B	1	20.17	20.17	215.22	0.000 7	1	23.25	23.25	60.93	0.004 4
AB	1	0.250 0	0.250 0	2.67	0.200 9	1	0.002 0	0.002 0	0.005 3	0.946 5
A^2	1	3.47	3.47	37.00	0.008 9	1	1.91	1.91	5.02	0.111 0
B^2	1	0.035 6	0.035 6	0.3794	0.581 5	1	0.001 6	0.001 6	0.004 2	0.952 4
Residual	3	0.281 1	0.093 7			3	1.14	0.381 5		
Cor total	8	157.68				8	233.64			

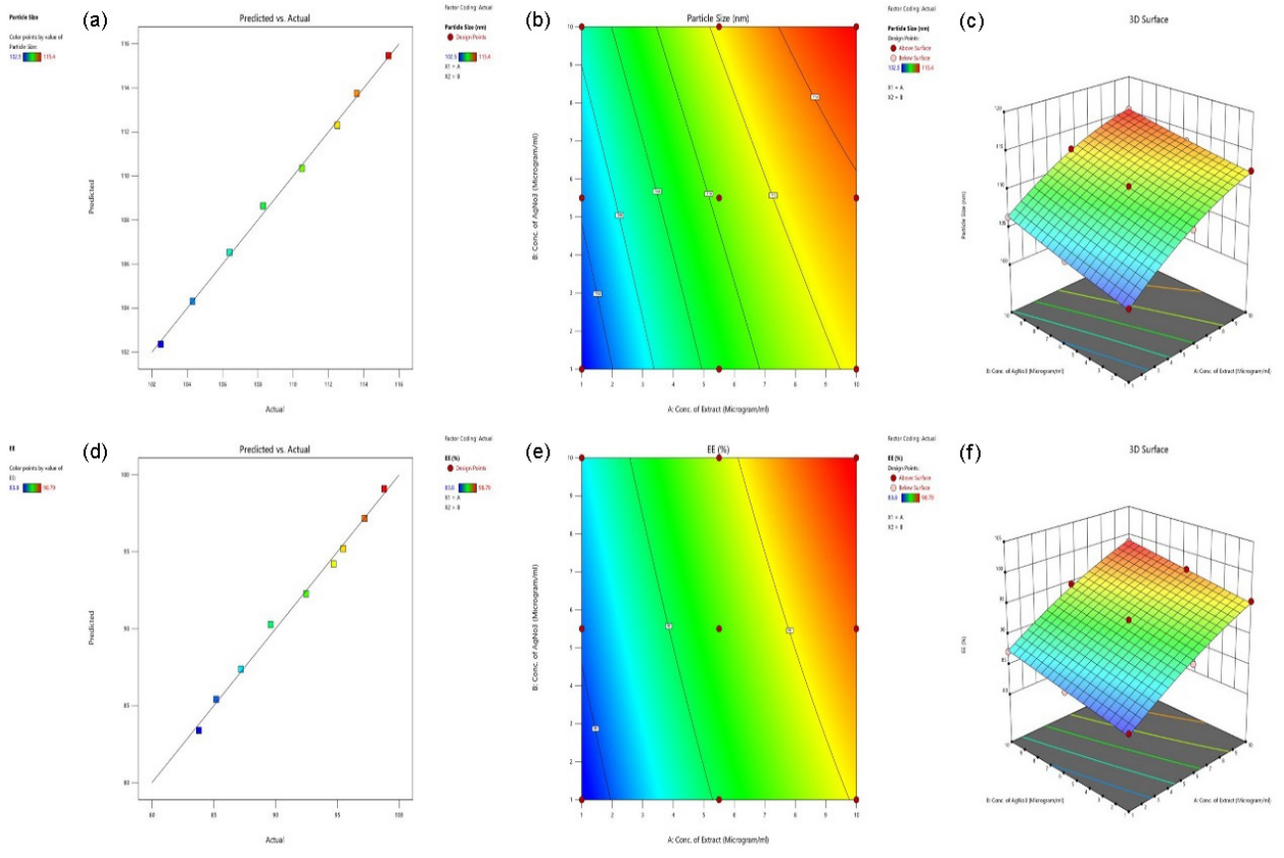

Fig. 1 (a) Predicted vs. actual plot, **(b)** 2D counter plot, and **(c)** 3D response surface plots of the selected model for particle size. **(d)** Predicted vs. actual plot, **(e)** 2D counter plot, and **(f)** 3D response surface plots of the selected model for percentage entrapment efficiency.

treated with $AgNO_3$. Both the AHL extract and the AH-AgNPs were examined using FT-IR spectroscopy. The FT-IR spectra of the AHL extract revealedvibrationstretchesat3296.70,2921.31,2855.12, 1 735.06, 1 043.51, 860.73, 704.24, and 660.66 cm^{-1}. The AH-AgNPs exhibited distinct peaks at 3 266.82, 2 975.62, 2 896.56, 1 648.84, 1 450.21, 1 085.73, 1 043.30, and 879.38 cm^{-1} (Fig. 2). The banding pattern of these groups is consistent with that of polyphenols, as demonstrated by Chen and Mu [45] and Chavan et al. [46]. The bands at 3 266.82 cm^{-1} and 3 296.70 cm^{-1} indicate O–H stretching vibrations of the phenolic group in the AH-AgNPs. The peaks at 2 896.56 and 2 921.31 cm^{-1} correspond to the C–H stretching of aromatic compounds in the AH-AgNPs. The vibration stretches at 1 648.84 and 1 735.06 cm^{-1} suggest the presence of an aromatic group in the AH-AgNPs. Notably, both the AHL and AH-AgNPs did not exhibit the peak at 1 511.92 cm^{-1}, which corresponds to the O–H bending of polyphenols. In the IR spectra, the AHL and AH-AgNPs showed C=O stretching vibrations at 1 085.73 and 1 043.30 cm^{-1}, respectively. The FT-IR analysis indicates that the phenolic and flavonoid compounds present in the AH-AgNPs play a crucial role in capping and stabilizing the nanoparticles [47]. Furthermore, the FT-IR spectra of the AH-AgNPs, both alone and when mixed with Carbopol, did not show significant differences, suggesting that the polyphenolic and flavonoid groups are retained in their original form within the gel formulation. This retention is vital for the stability and functionality of the nanoparticles, highlighting the effectiveness of the encapsulation process. The results of SEM revealed that the produced AH-AgNPs were spherical in shape (Fig. 3). Additionally, TEM confirmed that the synthesized AH-AgNPs were also spherical, with an average particle size of 10.08 ± 1.972 nm (Figs. 4(a)–4(d)). The average particle size was calculated using ImageJ software, and a detailed histogram is presented in Fig. 4(f). The crystalline nature of the AH-AgNPs is indicated by the ring-like diffraction pattern shown in Fig. 4(e) from the SAED image, consistent with previous observations by Bhinge et al. for silver nanoparticles synthesized using *Bryophyllum Pinnatum* extract [48]. Furthermore, the XRD pattern suggest that the AH-AgNPs are crystalline (Fig. 4(g)).

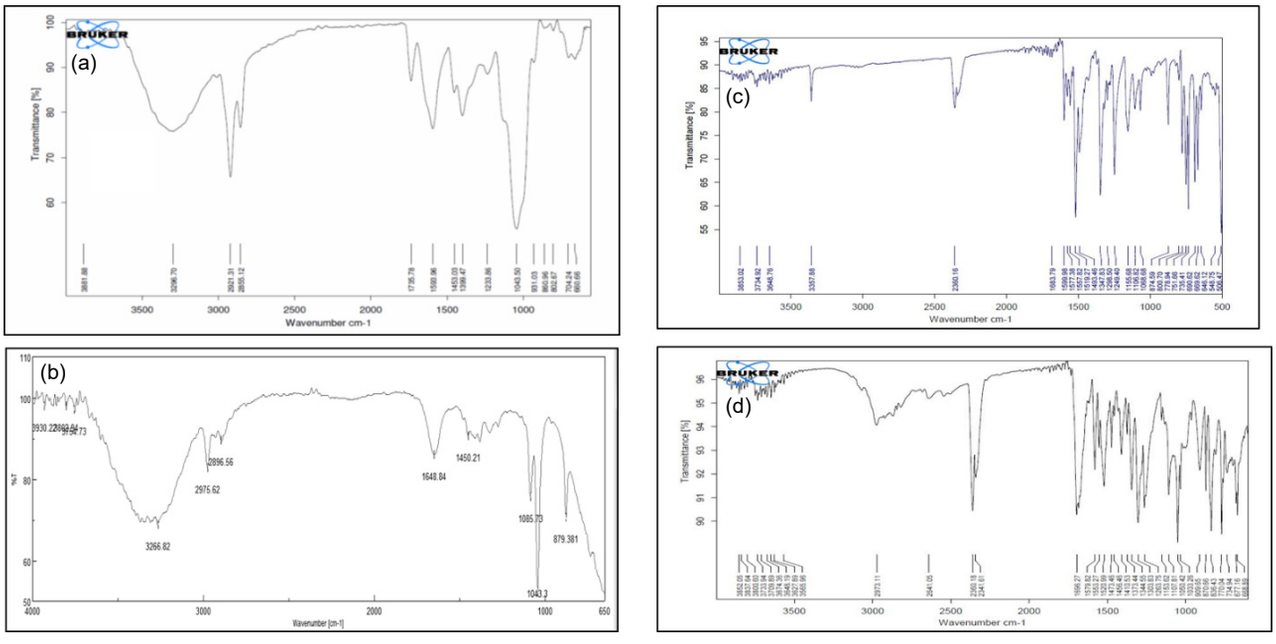

Fig. 2 FT-IR spectra of **(a)** the AHL extract, **(b)** pure AH-AgNPs synthesized from AHL, **(c)** Carbopol 940, and **(d)** The mixture of Carbopol 940 and AH-AgNPs.

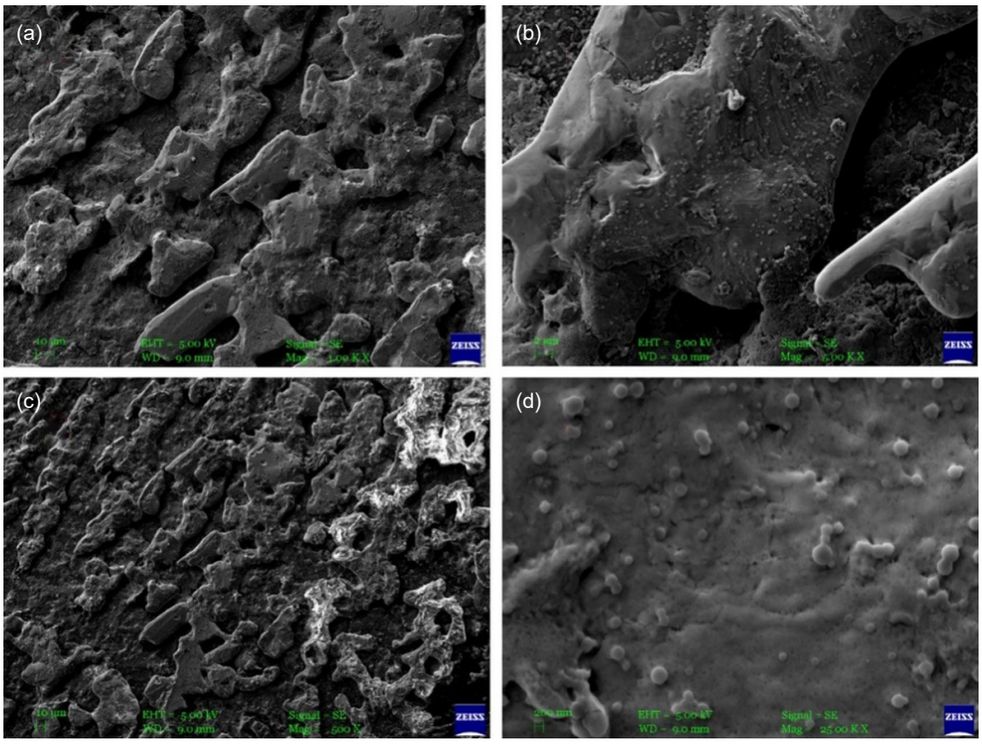

Fig. 3 SEM analysis of AH-AgNPs synthesized from AHL: Images captured at **(a)** 40 µm, **(b)** 2 µm, **(c)** 10 µm, and **(d)** 2 000 nm

Formulation of AH-AgNPs incorporated gel

The gel formulation was successfully prepared using Carbopol 940 as the gel base.

Evaluation of the gel

Color, appearance, and homogeneity

The control gel containing Carbopol 940 was translucent and colorless, while the gel formulation with AH-AgNPs exhibited a brownish hue. The AH-AgNPs gel was free of lumps and foreign particles, demonstrating its homogeneous nature.

pH and viscosity

The gel displayed a nearly neutral pH, ranging from 6.8 ± 0.2 to 7.1 ± 0.2. The viscosity of the gel

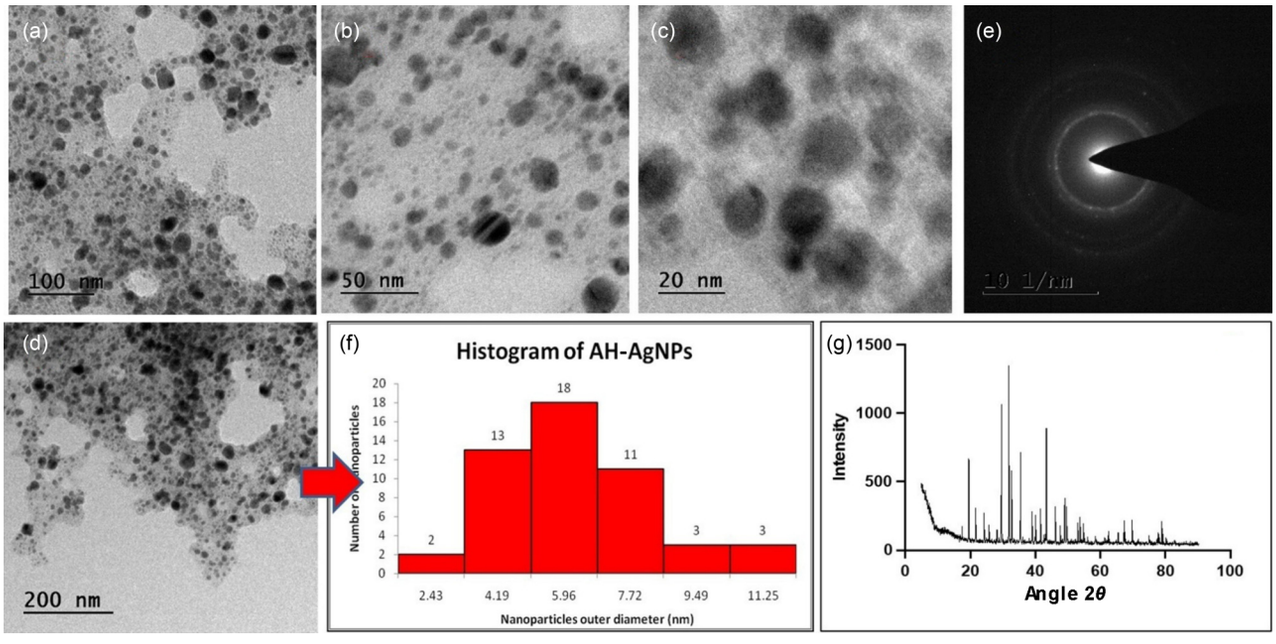

Fig. 4 TEM analysis of AH-AgNPs synthesized from AHL: **(a–e)** TEM images, **(f)** Histogram, and **(g)** XRD pattern.

measured 2 884 cp, compared to 3 047 cp for the marketed formulation (M). Viscosity is an important indicator of consistency, with the gel containing Carbopol 940 showing a viscosity closer to that of the marketed gel M. Detailed results are presented in Table 3.

Spreadability

Spreadability refers to the gel's ability to evenly cover a larger area upon application to the skin or affected area, ensuring uniformity and enhancing patient compliance. This property is critical for determining therapeutic effectiveness. The formulated gels demonstrated spreadability comparable to the marketed formulation, with gel A exhibiting superior spreadability compared to gel M. Detailed results are presented in Table 3.

Zeta potential

The formulation exhibited a high zeta potential, ranging from 31.40 to 36.45 mV (Table 3), indicating excellent stability. The gel loaded with AgNPs displayed adequate charge and mobility, effectively preventing nanoparticle aggregation. The negative zeta potential of the silver nanoparticle-loaded gel suggests robust stability against aggregation, as negatively charged particles repel each other in nanoparticulate solutions, ensuring their independence and integrity.

Extrudability

The ease of extrusion from the tube is essential for the gel's applicability. Highly viscous gels may be challenging to extrude, while low-viscosity gels may flow too quickly, necessitating a balance in consistency. The formulated gel demonstrated superior extrudability comparable to that of the marketed formulation. Results are summarized in Table 3.

Rheological investigations

As the shear rate increased, all formulations demonstrated a decrease in viscosity, indicating shear-thinning behavior that enhances the spreadability of the gels.

Steady shear properties

Figures 5(a) and 5(b) illustrate the relationship between shear stress and shear rate. As the shear rate increased, shear stress also increased, while the viscosity of the gel decreased, further confirming its shear-thinning behavior. Table 4 presents the derived values of yield stress (τ_0), consistency index (K), flow

Table 3 Evaluation of the AH-AgNPs gel compared to the marketed formulation.

Sr. No.	Batches	pH	Viscosity (cp)	Spreadability (cm^2/g)	Extruability	Zeta potential (mV)
1	AH-AgNPs gel	6.8 ± 0.2	2 884	0.25	32.12 ± 0.05	−31.40 ± 0.00
2	Silverex (STD)	7.1 ± 0.2	3 047	0.22	30.13 ± 0.18	−36.45 ± 0.00

index (n), and coefficient of determination (R^2) obtained from the graph.

The consistency index (K) ranged from 16.76 to 146.01 Pa·s, with gel formulation A exhibiting the lowest value and formulation M showing the highest. K represents the viscous behavior of the gel. A value of $n = 1$ indicates Newtonian fluid behavior, whereas a value of $n > 1$ suggests thickening behavior. The n values for the gels ranged from 0.24 to 0.39, indicating that the gel formulations displayed shear-thinning behavior upon shear stress, classifying them as non-Newtonian fluids. The R^2 values for the equations were greater than 0.971, indicating that the power law provided the best fit for the data. Additionally, K can also serve as a criterion for viscosity assessment [31, 49].

Frequency sweep test

A frequency sweep test offers a more direct correlation with the microstructure of gels compared to steady rheology, as it enables the examination of materials in their resting state without disturbing their structures [50]. The viscoelastic behavior of the gels is illustrated in Figs. 5(c) and 5(d) through a frequency sweep test conducted at 25 °C. The graph depicts the relationship between the elastic modulus (G') and the viscous modulus (G"). The data obtained from the frequency sweep test confirmed that the gels exhibited viscoelastic properties.

In vitro diffusion

The cumulative percentage of drug release (AH-AgNPs) after 8 h is presented in Table 5. The cumulative release was determined to be 83.42% ± 0.58% for the synthsized gel and 84.22% ± 0.61% for the marketed formulation (M).

Release kinetic study of AH-AgNPs

The data obtained from the release of AH-AgNPs from the gel formulation were analyzed using various kinetic equations, including zero-order, first-order, Higuchi model, and Korsmeyer–Peppas model. The

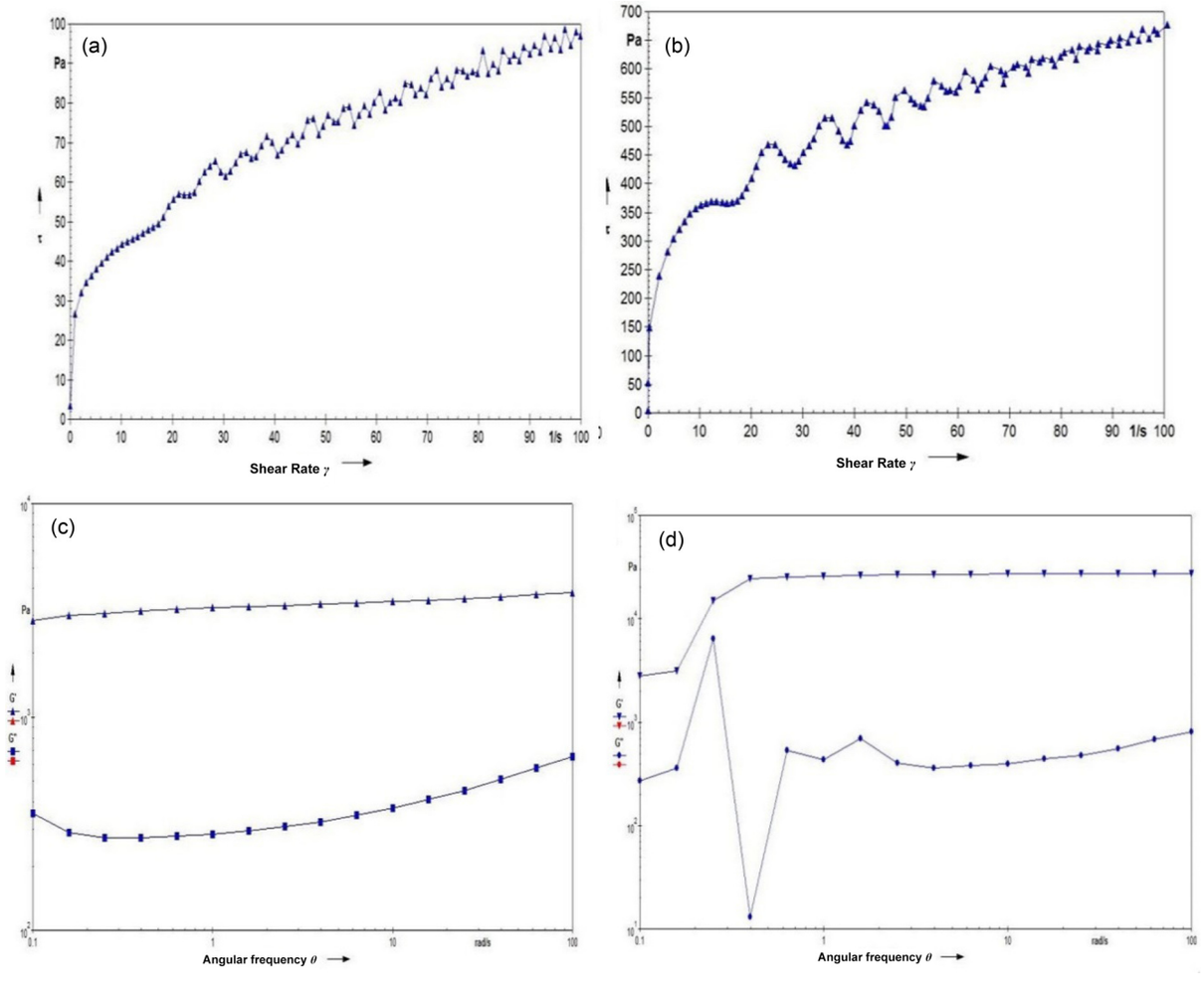

Fig. 5 Graph of shear stress (τ) versus shear rate (γ) for the AH-AgNPs gel formulation **(a)** and **(b)** the marketed formulation, M; frequency dependence data for the AH-AgNPs gel formulation **(c)** and **(d)** the marketed formulation, M at 37 °C.

Table 4 Yield stress, consistency index, flow index, and R^2 values for the AH-AgNP gel formulations and the marketed formulation, M.

Sr. No.	Formulation	Yield stress τ_0 (Pa)	Consistency index K (Pa·s)	Flow index (n)	R^2
1	AH-AgNPs gel	3.32	16.76	0.35 (shear thinning)	0.986
2	Silverex (STD)	145.09	145.09	0.23 (shear thinning)	0.987

Table 5 Cumulative percentage of drug release for the AH-AgNPs incorporated gel and the marketed formulation.

Time (min)	Cumulative amount permeated per cm² (%)	
	Marketed formulation	Prepared formulation
0	0	0
30	0.67% ± 0.13%	0.57% ± 0.03%
60	2.82% ± 0.23%	2.72% ± 0.14%
90	5.88% ± 0.02%	5.67% ± 0.38%
120	9.09% ± 0.28%	9.11% ± 0.45%
150	15.09% ± 0.025%	14.92% ± 0.30%
180	22.15% ± 0.73%	21.63% ± 0.43%
210	30.56% ± 0.52%	30.36% ± 0.52%
240	38.30% ± 0.84%	38.41% ± 0.65%
270	49.71% ± 0.50%	49.04% ± 0.70%
300	60.11% ± 0.90%	59.78% ± 0.52%
330	72.21% ± 0.36%	71.69% ± 0.82%
360	84.22% ± 0.61%	83.42% ± 0.58%

results presented in Table 6 indicate that the release of AH-AgNPs from the gel formulation follows zero-order kinetics, as evidenced by the higher R^2 associated with the zero-order kinetic model. Furthermore, the gel exhibited a higher R^2 value, suggesting a more linear release profile of the drug from the gel.

Stability

The gel formulation remained physically and chemically stable for over six months, exhibiting no observable changes in color, appearance, pH, or zeta potential of the AH-AgNPs gel formulations, even after this extended duration. The results of the stability studies are presented in Table 7.

Skin irritation test

Skin irritation studies indicated no abnormal effects on the denuded area of the selected rat. No redness, swelling, or dryness was observed in the treated area (Fig. 6). Both the AHL extract AH-AgNPs gel and the marketed gel (M) were determined to be safe, showing no potential for irritation.

Antimicrobial activity of AH-AgNP gel formulation

The antimicrobial activity was evaluated by measuring the diameter of the zone of inhibition. The results of testing the antibacterial activity of various formulations against selected pathogens are displayed in Table 8 and Fig. 7. The formulated gel demonstrated a larger zone of inhibition compared to the extract against the Gram-negative bacterium *E. coli*. Moderate activity was observed against *A. niger* and *S. aureus*, while the least activity was noted against *B. subtilis*. These results were statistically significant. Thus, the gel formulation, despite having a lower dose of silver, could serve as an effective alternative antimicrobial treatment for pathogenic diseases caused by antibiotic-resistant microbes.

Table 6 R^2 values for different equations and models.

Sr. No.	Formulation	Zero order	First-order R^2	Higuchi model	Korsmeyer–Pappas model
1.	AH-AgNPs gel	0.990	0.933	0.915	0.896
2.	Silverex (STD)	0.989	0.936	0.906	0.866

Table 7 Results of the stability studies.

Parameters	Sampling time (month)						
	0	1	2	3	4	5	6
Color	Brownish	Brownish	Brownish	Brownish	Brownish	Brownish	Brownish
Honogenesity	Homogeneous	Homogeneous	Homogeneous	Homogeneous	Homogeneous	Homogeneous	Homogeneous
pH	6.8 ± 0.2	6.5 ± 0.1	6.6 ± 0.4	6.4 ± 0.2	6.7 ± 0.1	6.5 ± 0.3	6.8 ± 0.3
Zeta potential (mV)	−31.40 ± 0.00	−31.82 ± 0.03	−31.52 ± 0.12	−31.36 ± 0.24	−31.42 ± 0.03	−31.37 ± 0.04	−31.41 ± 0.01

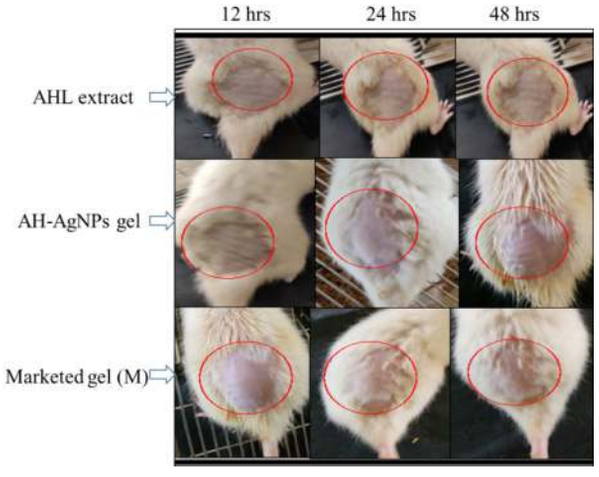

Fig. 6 Skin irritation study.

Table 8 Antibacterial activity of silver nanoparticles (AH-AgNPs) and AHL extract [values (mean ± SEM) represent the average of three experiments (n = 1 × 3)].

Bacterial strains	Inhibition zone (mm)		
	Plant extract (AHL)	AH-AgNPs	Marketed formulation
	Antimicrobial activity		
E. Coli	8.25 ± 0.45	16.59 ± 0.52	18.8 ± 0.34
B. Substalis	8.57 ± 0.87	19.83 ± 0.28	20.86 ± 0.23
S. Aureus	8.65 ± 0.85	16.23 ± 0.40	19.92 ± 0.12
	Antifungal activity		
A. Niger	8.02 ± 0.85	14.20 ± 0.64	20.6 ± 1.03

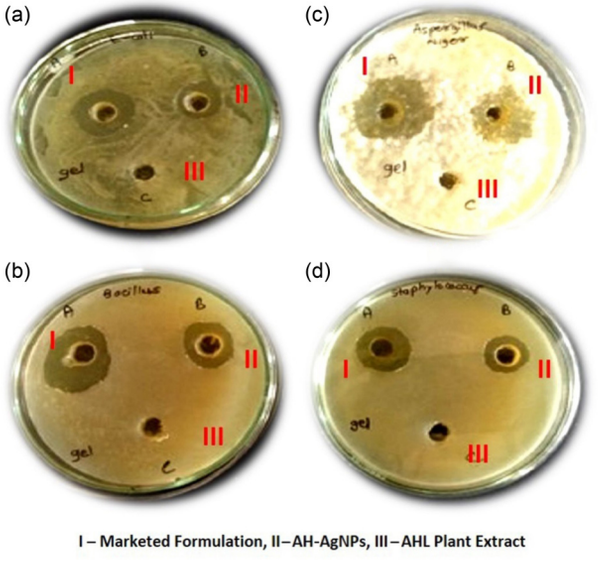

Fig. 7 Antimicrobial activity of the synthesized silver nanoparticles (AH-AgNPs) and *Artocarpus heterophyllus* leaf extract against *Escherichia coli* **(a)**, *Bacillus subtilis* **(b)**, *A. Niger* **(c)**, and *Staphylococcus aureus* **(d)**.

Silver nanoparticles exert their antimicrobial effect through several mechanisms, including protein inactivation, interference with DNA replication, and alteration of cell membrane permeability. They have been shown to bind to the bacterial cell wall, causing physical changes in the membrane, which ultimately leads to membrane damage and leakage of cellular contents [51]. The stronger antibacterial action observed against *E. coli* may be attributed to the difference in sensitivity and cell wall thicknessbetween gram-negative and gram-positive bacteria [52].

Conclusions

The development of a topical gel incorporating optimized AH-AgNPs synthesized from AHL extracts marks a significant achievement in nanomedicine. This study successfully demonstrated the formulation met stringent physicochemical criteria, including a smooth texture, viscosity suitable for topical application, and transparency. Despite containing a lower concentration of silver, the gel exhibited robust antimicrobial properties comparable to those of a commercially available formulation. Notably, it showed superior efficacy against *E. coli* when compared to the standard silver nitrate-based product, highlighting its potential as an effective treatment option for pathogenic infections. These findings underscore the promise of AH-AgNP-loaded gels in combating antibiotic-resistant microbes, suggesting their role in future biomedical applications. Further research could explore additional therapeutic benefits and optimize formulation parameters to enhance clinical utility and safety profiles.

CRediT Author Statement

Rohankumar R. Chavan: conceptualization, methodology, software, writing original draft preparation. **Mangesh A. Bhutkar:** visualization, investigation, software supervision, writing-reviewing and editing. **Somnath D. Bhinge & Vishal H. Thorat:** conceptualization, writing-reviewing and editing.

Acknowledgements

The authors are thankful to Dr. S. K. Mohite, Principal, Rajarambapu College of Pharmacy,

Kasegaon (Maharashtra) for providing the necessary facilities to carry out the research work.

Conflict of Interests

The author does not have any conflicts of interest.

Supporting Information

Supporting information to this article can be found online at https://doi.org/10.26599/NBE.2024.9290104.

References

[1] D. Blondeau, L. Roy, S. Dumont, et al. Physicians' and pharmacists' attitudes toward the use of sedation at the end of life: Influence of prognosis and type of suffering. *Journal of Palliative Care*, 2005, 21(4): 238−245. https://doi.org/10.1177/082585970502100402

[2] L. Zhang, F.X. Gu, J.M. Chan, et al. Nanoparticles in medicine: Therapeutic applications and developments. *Clinical Pharmacology & Therapeutics*, 2008, 83(5): 761−769. https://doi.org/10.1038/sj.clpt.6100400

[3] A. Yaqub, M. Rashid, S.A. Ditta, et al. *In vivo* Antioxidant potential of biogenic silver nanoparticles synthesized from *Psidium guajava* L. *Nano Biomedicine and Engineering*, 2023, 15(3): 225–238. https://doi.org/10.26599/NBE.2023.9290026

[4] F. Huang, X.Y. Cai, X.X. Hou, et al. A dynamic covalent polymeric antimicrobial for conquering drug-resistant bacterial infection. *Exploration*, 2022, 2(5): 20210145. https://doi.org/10.1002/exp.20210145

[5] N. Madubuonu, S.O. Aisida, I. Ahmad, et al. Bio-inspired iron oxide nanoparticles using Psidium guajava aqueous extract for antibacterial activity. *Applied Physics A*, 2020, 126(1): 72. https://doi.org/10.1007/s00339-019-3249-6

[6] S. Das, A. Das, A. Maji, et al. A compact study on impact of multiplicative Streblus asper inspired biogenic silver nanoparticles as effective photocatalyst, good antibacterial agent and interplay upon interaction with human serum albumin. *Journal of Molecular Liquids*, 2018, 259: 18−29. https://doi.org/10.1016/j.molliq.2018.02.111

[7] E.C. Njagi, H. Huang, L. Stafford, et al. Biosynthesis of iron and silver nanoparticles at room temperature using aqueous sorghum bran extracts. *Langmuir*, 2011, 27(1): 264−271. https://doi.org/10.1021/la103190n

[8] R. Joseph, A. Naugolny, M. Feldman, et al. Cationic pillararenes potently inhibit biofilm formation without affecting bacterial growth and viability. *Journal of the American Chemical Society*, 2016, 138(3): 754−757. https://doi.org/10.1021/jacs.5b11834

[9] H.C. Flemming, J. Wingender, U. Szewzyk, et al. Biofilms: An emergent form of bacterial life. *Nature Reviews Microbiology*, 2016, 14(9): 563−575. https://doi.org/10.1038/nrmicro.2016.94

[10] J.M. Ahn, H.J. Eom, X.Y. Yang, et al. Comparative toxicity of silver nanoparticles on oxidative stress and DNA damage in the nematode, Caenorhabditis elegans. *Chemosphere*, 2014, 108: 343−352. https://doi.org/10.1016/j.chemosphere.2014.01.078

[11] L.L. Maurer, J.N. Meyer. A systematic review of evidence for silver nanoparticle-induced mitochondrial toxicity. *Environmental Science: Nano*, 2016, 3(2): 311−322. https://doi.org/10.1039/c5en00187k

[12] O.S. Adeyemi, E.O. Shittu, O.B. Akpor, et al. Silver nanoparticles restrict microbial growth by promoting oxidative stress and DNA damage. *EXCLI Journal*, 2020, 19: 492−500. https://doi.org/10.17179/excli2020-1244

[13] S.K. Kailasa, T.J. Park, J.V. Rohit, et al. Antimicrobial activity of silver nanoparticles. In: Nanoparticles in Pharmacotherapy. Amsterdam: Elsevier, 2019: 461–484. https://doi.org/10.1016/b978-0-12-816504-1.00009-0

[14] K. Abdali, K.H. Abass, E. Al-Bermany, et al. Morphological, optical, electrical characterizations and anti- escherichia coli bacterial efficiency (AECBE) of PVA/PAAm/PEO polymer blend doped with silver NPs;. *Nano Biomedicine and Engineering*, 2022, 14(2): 114−122. https://doi.org/10.5101/nbe.v14i2.p114-122

[15] F. Andrade, C. Jenipher, N. Gurav, et al. Endophytic fungus colletotrichum siamense derived silver nanoparticles: Biomimetic synthesis, process optimization and their biomedical applications. *Journal of Inorganic and Organometallic Polymers and Materials*, 2024. https://doi.org/10.1007/s10904-024-03235-9

[16] S.V. Kadam, C.S. Magdum, S.R. Kane, et al. Investigation of therapeutic potential of biosynthesized silver and gold nanoparticles using extract of *Wrightia tinclooria*. *Nanoscience & Nanotechnology-Asia*, 2023, 14(2): e101023222010. https://doi.org/10.2174/0122106812264073230929170021

[17] M.A. Bhutkar, D.S. Randive, S.D. Bhinge, et al. Development of gold, silver, and iron nanoparticles using isolated berberine: Its characterization and antimicrobial and cytotoxic activities against COLO320DM and Hela cells. *Gold Bulletin*, 2022, 55(1): 93−103. https://doi.org/10.1007/s13404-022-00309-9

[18] R.R. Chavan, S.D. Bhinge, M.A. Bhutkar, et al. Green synthesis of silver and iron nanoparticles using fresh plant extracts of blumeaeriantha dc: evaluation of its hair growth promoting activity and partial characterization. *Journal of Cosmetic Dermatology*, 2020, 20(04): 1283−1297. https://doi.org/10.1111/jocd.13713

[19] K.P. Shejawal, D.S. Randive, S.D. Bhinge, et al. Green synthesis of silver and iron nanoparticles of isolated proanthocyanidin: Its characterization, antioxidant, antimicrobial, and cytotoxic activities against COLO320DM and HT29. *Journal of Genetic Engineering and Biotechnology*, 2020, 18(1): 43. https://doi.org/10.1186/s43141-020-00058-2

[20] D.A. Helal, D.A. El-Rhman, S.A. Abdel-Halim, et al. Formulation and evaluation of fluconazole topical gel. *International Journal of Pharmacy and Pharmaceutical Sciences*, 2012, 4(SUPPL. 5): 176–183.

[21] H.J. Rathod, D.P. Mehta. A review on pharmaceutical gel. *International Journal of Pharmaceutical Sciences*, 2015, 1(1): 33−47.

[22] R.M.P. Singh, A. Kumar, K. Pathak. Thermally triggered mucoadhesive *in situ* gel of loratadine: β-cyclodextrin complex for nasal delivery. *AAPS PharmSciTech*, 2013, 14(1): 412−424. https://doi.org/10.1208/s12249-013-9921-9

[23] R. Said dos Santos, H.C. Rosseto, J. Bassi da Silva, et al. The effect of carbomer 934P and different vegetable oils on physical stability, mechanical and rheological properties of emulsion-based systems containing propolis. *Journal of Molecular Liquids*, 2020, 307: 112969. https://doi.org/10.1016/j.molliq.2020.112969

[24] M.S. Alam, A. Garg, F.H. Pottoo, et al. Gum ghatti mediated, one pot green synthesis of optimized gold nanoparticles: Investigation of process-variables impact using box-behnken based statistical design. *International Journal of Biological Macromolecules*, 2017, 104: 758−767. https://doi.org/10.1016/j.ijbiomac.2017.05.129

[25] Z.Z. Ge, M.Y. Yang, Y.L. Wang, et al. Preparation and evaluation of orally disintegrating tablets of taste masked phencynonate HCl using ion-exchange resin. *Drug Development and Industrial Pharmacy*, 2015, 41(6):

934−941. https://doi.org/10.3109/03639045.2014.914529
[26] S.D. Bhinge, S.P. Kamalakar, D.S. Randive, et al. Statistically developed Proanthocyanidin loaded PLAROsomes for improved therapy of pharmacological activity. *European Journal Pharmaceutics and Biopharmaceutics*, 2024, 126(6): 2300218. https://doi.org/10.1002/ejlt.202300218
[27] S.T. Jadhav, V.R. Salunkhe, S.D. Bhinge, et al. Development and evaluation of imiquimod-loaded nanoemulsion-based gel for the treatment of skin cancer. *Future Journal of Pharmaceutical Sciences*, 2024, 10(1): 93. https://doi.org/10.1186/s43094-024-00660-y
[28] N. Prabhu, D.T. Raj, K. Yamuna Gowri, et al. Synthesis of silver phyto nanoparticles and their antibacterial efficacy. *Digest Journal of Nanomaterials and Biostructures*, 2010, 5(1): 185−189.
[29] M. Singhal, L. Loveleen, R. Manchanda, et al. Design, synthesis and optimization of silver nanoparticles using Azadirachta indica bark extract and its antibacterial application. *Journal of Agriculture and Food Research*, 2024, 16: 101088. https://doi.org/10.1016/j.jafr.2024.101088
[30] S. Mathew, C.P. Victório, J. Sidhi, et al. Biosynthesis of silver nanoparticle using flowers of Calotropis gigantea (L.) W.T. Aiton and activity against pathogenic bacteria. *Arabian Journal of Chemistry*, 2020, 13(12): 9139−9144. https://doi.org/10.1016/j.arabjc.2020.10.038
[31] J.C. Ontong, S. Singh, O.F. Nwabor, et al. Potential of antimicrobial topical gel with synthesized biogenic silver nanoparticle using Rhodomyrtus tomentosa leaf extract and silk sericin. *Biotechnology Letters*, 2020, 42(12): 2653−2664. https://doi.org/10.1007/s10529-020-02971-5
[32] K. Singh, M. Panghal, S. Kadyan, et al. Evaluation of antimicrobial activity of synthesized silver nanoparticles using *Phyllanthus amarus* and *Tinospora cordifolia* medicinal plants. *Journal of Nanomedicine & Nanotechnology*, 2014, 5(6): 1000250. https://doi.org/10.4172/2157-7439.1000250
[33] M. Shukr, G.F. Metwally. Evaluation of topical gel bases formulated with various essential oils for antibacterial activity against methicillin- resistant *Staphylococcus aureus*. *Tropical Journal of Pharmaceutical Research*, 2014, 12(6): 877. https://doi.org/10.4314/tjpr.v12i6.3
[34] G. Misal, V. Dixit, V. Gulkari. Formulation and evaluation of herbal gel. *Indian Journal of Natural Products and Resources*, 2012, 3(4): 501−505.
[35] Sandhu, K. S., Singh, N., Kaur, M. Characteristics of the different corn types and their grain fractions: Physicochemical, thermal, morphological, and rheological properties of starches. *Journal of Food Engineering*, 2004, 64(1): 119–127. https://doi.org/10.1016/j.jfoodeng.2003.09.023
[36] S. Park, M.G. Chung, B. Yoo. Effect of octenylsuccinylation on rheological properties of corn starch pastes. *Starch*, 2004, 56(9): 399−406. https://doi.org/10.1002/star.200300274
[37] E.J. Ricci, M.V.L.B. Bentley, M. Farah, et al. Rheological characterization of Poloxamer 407 lidocaine hydrochloride gels. *European Journal of Pharmaceutical Sciences*, 2002, 17(3): 161−167. https://doi.org/10.1016/S0928-0987(02)00166-5
[38] A. Prusty, P. Parida. Development and evaluation of gel incorporated with biogenically synthesised silver nanoparticles. *Journal of Applied Biopharmaceutics and Pharmacokinetics*, 2015, 3(1): 1−6. https://doi.org/10.14205/2309-4435.2015.03.01.1
[39] S. Dash, P.N. Murthy, L. Nath, et al. Kinetic modeling on drug release from controlled drug delivery systems. *Acta Poloniae Pharmaceutica*, 2010, 67(3): 217−223.
[40] N. Mahendran, B. Anand, M. Rajarajan, et al. Green synthesis, characterization and antimicrobial activities of silver nanoparticles using Cissus quadarangularis leaf extract. *Materials Today: Proceedings*, 2022, 49: 2620−2623. https://doi.org/10.1016/j.matpr.2021.08.043
[41] Proceedings of the International Conference on Harmonisation. Geneva: 1993. Oct, ICH QIA. Stability testing of new drug substances and products.
[42] D. Kumar, N. Jain, N. Gulati, et al. Nanoparticles laden *in situ* gelling system for ocular drug targeting. *Journal of Advanced Pharmaceutical Technology & Research*, 2013, 4(1): 9. https://doi.org/10.4103/2231-4040.107495
[43] E. Urnukhsaikhan, B.E. Bold, A. Gunbileg, et al. Antibacterial activity and characteristics of silver nanoparticles biosynthesized from *Carduus crispus*. *Scientific Reports*, 2021, 11: 21047. https://doi.org/10.1038/s41598-021-00520-2
[44] K.Y. Yong, M.S. Abdul Shukkoor. *Manilkara zapota*: A phytochemical and pharmacological review. *Materials Today: Proceedings*, 2020, 29: 30–33. https://doi.org/10.1016/j.matpr.2020.05.688
[45] C.-X. Chen, S. Mu. The electrochemical preparation of polyphenol with conductibility. *Chinese Journal of Polymer Science*, 2002, 20(4): 309–316.
[46] R.R. Chavan, S.D. Bhinge, M.A. Bhutkar, et al. Characterization, antioxidant, antimicrobial and cytotoxic activities of green synthesized silver and iron nanoparticles using alcoholic *Blumea eriantha* DC plant extract. *Materials Today Communications*, 2020, 24: 101320. https://doi.org/10.1016/j.mtcomm.2020.101320
[47] N.J. Reddy, D. Nagoor Vali, M. Rani, et al. Evaluation of antioxidant, antibacterial and cytotoxic effects of green synthesized silver nanoparticles by Piper longum fruit. *Materials Science and Engineering: C*, 2014, 34: 115−122. https://doi.org/10.1016/j.msec.2013.08.039
[48] S.D. Bhinge, D. Pratiksha, B.M. Anil, et al. Facile synthesis and surface characterization of platinum and gold bimetallic nanoparticles prepared using hydroalcoholic extract of bryophyllum pinnatum: Enhancing efficacy against breast cancer. *Inorganic Chemistry Communications*, 2024, 165: 112555. https://doi.org/10.1016/j.inoche.2024.112555
[49] M. Sikora, S. Kowalski, P. Tomasik, et al. Rheological and sensory properties of dessert sauces thickened by starch–xanthan gum combinations. *Journal of Food Engineering*, 2007, 79(4): 1144−1151. https://doi.org/10.1016/j.jfoodeng.2006.04.003
[50] M.P. Mishra, R.N. Padhy. Antibacterial activity of green silver nanoparticles synthesized from Anogeissus acuminata against multidrug resistant urinary tract infecting bacteria *in vitro* and host-toxicity testing. *Journal of Applied Biomedicine*, 2018, 16(2): 120−125. https://doi.org/10.1016/j.jab.2017.11.003
[51] B. Khalandi, N. Asadi, M. Milani, et al. A review on potential role of silver nanoparticles and possible mechanisms of their actions on bacteria. *Drug Research*, 2016, 67(2): 70−76. https://doi.org/10.1055/s-0042-113383
[52] Y.A. Qing, L. Cheng, R.Y. Li, et al. Potential antibacterial mechanism of silver nanoparticles and the optimization of orthopedic implants by advanced modification technologies. *International Journal of Nanomedicine*, 2018, 13: 3311−3327. https://doi.org/10.2147/ijn.s165125